FED-Vol. 243
MD-Vol. 78

RHEOLOGY AND FLUID MECHANICS OF NONLINEAR MATERIALS — 1997 —

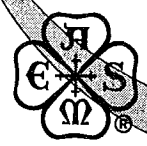

Edited by
S. G. ADVANI
D. A. SIGINER

1997 ASME INTERNATIONAL MECHANICAL ENGINEERING CONGRESS AND EXPOSITION

FED-Vol. 243/MD-Vol. 78, Rheology and Fluid Mechanics
of Nonlinear Materials
ASME 1997

A FINITE VOLUME COLOCATED-MESH METHOD FOR THE PREDICTION OF NON-NEWTONIAN FLUID FLOW

Paulo J. Oliveira
Departamento de Engenharia Electromecânica
Universidade da Beira Interior
Rua Marquês D'Ávila e Bolama
6200 Covilhã, Portugal

Fernando T. Pinho[1]
Departamento de Engenharia Mecânica
e Gestão Industrial
Faculdade de Engenharia, Universidade do Porto
Rua dos Bragas, 4099 Porto Codex, Portugal

Gilberto A. Pinto
Departamento de Engenharia Química
Instituto Superior de Engenharia do Porto
Rua de São Tomé, 4200 Porto Codex, Portugal

ABSTRACT

This paper reports the development of a methodology for calculating the flow of upper convected Maxwell fluids using a finite-volume based method. The algorithm was developed for a general non-orthogonal collocated grid, and the pressure-velocity-stress coupling was addressed by a special interpolation technique inspired by Rhie and Chow's (1982) method. The differencing schemes are second order accurate and calculations were carried on for a two-dimensional entry channel flow in order to assess the performance of the method. The interpolation technique specially devised for the stresses was found to work well and the results of the simulation compared favourably with those of the literature (Eggleton et al, 1996). Convergence was attained for Deborah and Reynolds numbers identical to those reported in the literature for a similar flow problem using other numerical methods.

Viscoelasticity was responsible for the development of very intense normal stresses, which were tractive in the wall region. As a consequence the viscoelastic fluid was forced to move away from the wall, in a more intense way than with Newtonian fluids, thus reducing locally the shear rates and the role of viscosity in redeveloping the flow.

KEYWORDS: finite-volume, collocated grids, non-orthogonal coordinates, Upper Convected Maxwell model, slip- stick flow

1. INTRODUCTION

Finite-volume methods are known to be advantageous in terms of space and time requirements for the calculation of fluid flow, as well as for reasons of numerical stability, in comparison to finite-element methods, Huang et al (1996). Various such finite volume methods have been developed and used in Newtonian fluid mechanics from the late sixties, as can be assessed by any specialised book on the subject (Versteeg and Malalasekera, 1995).

In spite of its many advantages, finite-volume methods were not used in the computation of non-Newtonian viscoelastic fluid flows for quite a long time but, recently, various research groups have started developing finite-volume based algorithms.

One recent numerical work based on the finite-volume approach was the investigation of the flow of an Upper Convected Maxwell model fluid around a circular cylinder by Hu and Joseph (1990). A staggered orthogonal grid and the SIMPLER (Semi-Implicit Method for Pressure Linked Equations Revised) algorithm were used and adapted for calculating the stress equation. The inertia terms of the momentum equation were neglected because the calculations were limited to low Reynolds number flows, of the order of 0.4 to 10, with convergence attained for Weissenberg numbers up to 10.

Inclusion of inertia terms in the momentum equation is required for higher Reynolds number flows, but may have consequences on the convergence rate at low Reynolds number flows. Hence, it is important to include inertia in the development of general algorithms, as done by Yoo and Na (1991) in their predictions of the sudden contraction. As Hu and Joseph, these authors also considered first order interpolation schemes, which are known to cause numerical diffusion whenever the flow is not aligned with the grid orientation (Raithby, 1976). The use of staggered grids has also been the normal practice in the above works, as well as in other instances of finite-volume based calculations of non-Newtonian fluids (Sasmal, 1995, Gervang and Larsen, 1991 and Xue et al, 1995).

The advantage of a formulation based on colocated non-orthogonal grids for handling handling the flow of non-Newtonian fluids in complex geometries has been recently recognized by Huang et al (1996), who used a so-called non-structured method for predicting the flow of Phan-Thien-Tanner fluids in eccentric bearings, but the inertia terms of the momentum equation were neglected again.

The use of simple non-linear models, such as the Upper Convected Maxwell (UCM) equations can only partially predict real fluid rheology, but they are very challenging models from the

[1] to whom all correspondence should be addressed

numerical point of view, because of their singularities in sharp boundaries. Thus, they are espécially adequate for developing accurate and robust numerical methods that can be upgraded later to more realistic constitutive equations. Indeed, it is generally accepted (eg. Huang et al, 1996) that the UCM equations pose the most severe numerical difficulties compared with other constitutive differential models, and so a good numerical method for the UCM is expected to work well with the other models.

The finite-volume method is applied to the simulation of viscoelastic entry flow into a 2-D plane channel. Here, two options may be taken: either a uniform velocity profile is imposed right at the channel entrance, or, following Eggleton et al (1996), an initial unbounded region is considered upstream, where the flow is allowed to relax to adapt itself to the channel entrance conditions. This last option was adopted here because it is less demanding in numerical terms and it is a situation in which the stresses in the fluid are closer to what happens in a real entry flow. Few authors (see Gaidos and Darby, 1988 and references within) tried the former problem, mainly with view to study possible occurence of bifurcation points in the solution. The finite-element meshes were very coarse (often only 3 elements accross the channel width) thus reducing the numerical problems. Even so, Gaidos and Darby (1988) were obliged to impose a piecewise continuous polynomial which would make a smooth transition between the uniform velocity and the zero value at the wall singularity; thus the imposed inlet velocity profile was only an approximation to the plug profile.

The objective of this paper is to further advance finite-volume based numerical methods for predicting non-Newtonian flows and to include non-orthogonal colocated grids and second order accurate interpolation schemes. A non-linear constitutive model, the White-Metzner constitutive equation, is adopted and in the next section the equations are presented and their discretization outlined. Then, the numerical method, the interpolation schemes, the methodology developed to address the pressure-velocity-stress coupling and the definition of boundary conditions are presented and discussed. The numerical procedure is then applied to investigate numerically the two-dimensional Poiseuille entry flow, the inverse configuration relative to the well-known stick-slip case and which may thus be called the slip-stick flow.

2. GOVERNING EQUATIONS

The basic equations are those for three-dimensional, incompressible and isothermal laminar flow of an upper convected Maxwell model fluid, hereafter referred as the UCM fluid. Unless otherwise stated or for outlined indices, the summation convention for repeated indices will apply to either Cartesian components (*i, j, ...*) or non-Cartesian (*l, m, ...*) directions.

The continuity equation is

$$\frac{\partial u_i}{\partial x_i} = 0 \tag{1}$$

and the momentum conservation equation is given by

$$\frac{\partial \rho u_i}{\partial t} + \frac{\partial}{\partial x_j}\left(\rho u_i u_j\right) = -\frac{\partial p}{\partial x_i} + \frac{\partial \tau_{ij}}{\partial x_j} + \rho g_i \tag{2}$$

where the extra stress tensor τ_{ij} is defined by the UCM constitutive equation

$$\tau_{ij} + \lambda \tau_{(1)ij} = \eta\left[\frac{\partial u_i}{\partial x_j} + \frac{\partial u_j}{\partial x_i}\right] - \frac{2}{3}\eta \frac{\partial u_k}{\partial x_k}\delta_{ij} \tag{3}$$

The last term on the rhs of the constitutive equation is zero for incompressible fluids, such as those analysed here, but it is kept because it is not exactly zero in the numerical approximation and improves the convergence rate. In (3) $\tau_{(1)ij}$ denotes Oldroyd's upper convected derivative of τ_{ij} given by

$$\tau_{(1)ij} = \frac{\partial \tau_{ij}}{\partial t} + u_k \frac{\partial \tau_{ij}}{\partial x_k} - \tau_{kj}\frac{\partial u_i}{\partial x_k} - \tau_{ik}\frac{\partial u_j}{\partial x_k} \tag{4}$$

The mass and momentum conservation equations and the constitutive equation obey the principle of invariance and are written for an orthogonal coordinate system (x_1,x_2,x_3). Their discretization on a general computational finite-volume mesh composed of non-orthogonal six-faced cells requires their prior transformation to a general non-orthogonal coordinate system (ξ_1, ξ_2, ξ_3) (see Fig. 1) and it is advantageous from a numerical point of view (Peric, 1985) to write them in a strong conservation form to impose conservation of all quantities in the final algebraic equations. The required transformation rules are

$$\frac{\partial}{\partial t} = \frac{1}{J}\frac{\partial}{\partial t} J$$
$$\frac{\partial}{\partial x_i} = \frac{1}{J}\frac{\partial}{\partial \xi_l}\beta_{li} \tag{5}$$

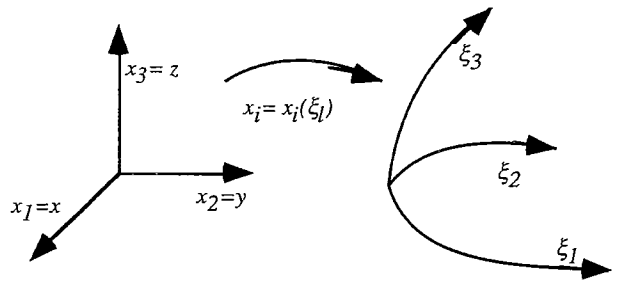

Figure 1- Schematic representation of the transformation of a rectangular Cartesian coordinate system to a non-orthogonal coordinate system which follows the mesh lines.

In the discretised equations the Jacobian J will be represented by cell volume V_P and the metric coefficients b_{li} by areas B_{li} (i-component of area vector along direction l, calculated at cell faces f or at cell centres P). The derivatives $\partial/\partial\xi_l$ will simply be represented by differences along direction l. After applying the rules of transformation (5) to Eqs. (1) to (4), these can be written in compact form, as follows:

- continuity

$$\frac{\partial}{\partial \xi_l}\left(\rho \beta_{lj} u_j\right) = 0 \tag{6}$$

- momentum

$$\frac{\partial}{\partial t}\left(J\rho u_i\right)+\frac{\partial}{\partial \xi_l}\left(\rho\beta_{lj}u_j u_i\right)=-\beta_{li}\frac{\partial p}{\partial \xi_l}+\frac{\partial}{\partial \xi_l}\left(\beta_{lj}\tau_{ij}\right)+J\rho g_i \quad (7)$$

- constitutive equation

$$J\tau_{ij}+\lambda\frac{\partial}{\partial t}\left(J\tau_{ij}\right)+\lambda\frac{\partial}{\partial \xi_l}\left(\beta_{lk}u_k\tau_{ij}\right)=\eta\left[\beta_{lj}\frac{\partial u_i}{\partial \xi_l}+\beta_{li}\frac{\partial u_j}{\partial \xi_l}\right]+$$

$$\lambda\left[\left(\beta_{lk}\tau_{kj}\right)\frac{\partial u_i}{\partial \xi l}+\left(\beta_{lk}\tau_{ki}\right)\frac{\partial u_j}{\partial \xi_l}\right]-\frac{2}{3}\eta\beta_{lk}\frac{\partial u_k}{\partial \xi_l}\delta_{ij} \quad (8)$$

In Eq. (7) the terms which will be dealt with implicitly in the numerical procedure are written on the lhs. It is well known that some diffusion can be very efficient in promoting the stability of finite-volume schemes when applied to transport equations, and since viscous diffusion is not explicitly present in Eq. (7) it was decided to add and subtract a normal diffusion term to it. This procedure departs from usual practice in non-Newtonian calculations, where the stress term is splitted into viscous and elastic contributions, and the viscous contribution is made to appear explicitly in the momentum equation. The two procedures may lead to analogous equations in some instances, but it should be noted that here the inclusion of the normal viscous term is just a numerical trick, based on experience gained in Newtonian flow calculations with the deferred correction approach (Khosla and Rubin, 1974) and computation of turbulent flows with the Reynolds-stress model (Basara and Younis, 1995). Eq. (7) is then substituted by Eq. (9) (l= l and no summation over subscript l)

$$\frac{\partial}{\partial t}\left(J\rho u_i\right)+\frac{\partial}{\partial \xi_l}\left(\rho\beta_{lj}u_j u_i\right)-\frac{\partial}{\partial \xi_l}\left(\frac{\eta}{J}\beta_{lj}\beta_{lj}\frac{\partial u_i}{\partial \xi_l}\right)=$$

$$-\beta_{li}\frac{\partial p}{\partial \xi_l}+\frac{\partial}{\partial \xi_l}\left(\beta_{lj}\tau_{ij}\right)+J\rho g_i-\frac{\partial}{\partial \xi_l}\left(\frac{\eta}{J}\beta_{lj}\beta_{lj}\frac{\partial u_i}{\partial \xi_l}\right) \quad (9)$$

in which all terms in the lhs are implicitly dealt with (incorporated into the coefficients) and those in the rhs are treated explicitly (incorporated into the source term) as explained hereafter. More details on this can be found in Pinto (1996).

3. NUMERICAL METHOD

3.1 Discretization of the equations

The calculation domain is divided into cells and Eqs. (6), (8) and (9) are volume-integrated in each cell to ensure a conservative discretization. This is accomplished via Gauss' theorem, as explained in Patankar (1980), and the discretization is performed with some differencing scheme applied to a universe of nodes constituted by those located at the centre of the cells and at the centre of their faces.

The discretised mass conservation Eq. (6) is required for the calculation of the pressure and becomes

$$\sum_{\mathrm{f}}^{6}(-1)^{\mathrm{f}}F_{\mathrm{f}}=0 \quad (10)$$

where the $(-1)^{\mathrm{f}}$ is used to yield positive outgoing convective fluxes F_{f}, calculated as

$$F_{\mathrm{f}}=\sum_{j}\left(\rho B_{\mathrm{f}j}\tilde{u}_j\right)_{\mathrm{f}} \quad (11)$$

with face index f = 1 to 6 for w, e, s, n, b and t, where compass notation is used.

The momentum Eq. (9) can be casted under the common linearised form for the velocity component u_i

$$\left(\frac{\rho V_{\mathrm{P}}}{\delta t}+a_o S_P\right)u_{i-\mathrm{p}}=\sum a_{\mathrm{f}}u_{i-\mathrm{f}}+S_{u_i}+\frac{\rho V_{\mathrm{P}}}{\delta t}u^{o}_{i-\mathrm{P}} \quad (12\ a)$$

where

$$a_o\equiv\sum a_{\mathrm{f}} \quad (12\ b)$$

For Newtonian fluids the neighbour terms (f) originate in the convective and diffusive contributions in the original equations with (f) standing for the near neighbour cells (W,E,S,N,B,T for f=1 to 6). Here, the diffusion of momentum coming through the constitutive equation is treated explicitly and it is the added diffusion term on the lhs of Eq. (9) which gives rise to the diffusion contribution to coefficients a_{f} An identical diffusion term is added to the rhs of Eq. (9), leading to terms $a_{\mathrm{f}}^{D}\,u_{i\text{-}nb}$, that go to the source S_{ui} of the momentum equation, generally given by:

$$S_{u_i}=S_{u_i-pressure}+S_{u_i-gravity}+S_{u_i-stress}+S^{D}_{u_i}+\sum a_{\mathrm{ff}}u_{i-\mathrm{ff}} \quad (13)$$

with the pressure, gravity and stress field quantities represented by $S_{ui\text{-}pressure}$, $S_{ui\text{-}gravity}$ and $S_{ui\text{-}stress}$, respectively. These source terms are readily obtained from Eq. (9), and are

$$S_{u_i-pressure}=-\sum_{l=1}^{3}B^{\mathrm{P}}_{li}\left[\Delta p\right]^{\mathrm{P}}_{l} \quad (14)$$

$$S_{u_i-gravity}=\rho g_i V_{\mathrm{P}} \quad (15)$$

$$S_{u_i-stress}=\sum_{\mathrm{f}}(-1)^{\mathrm{f}}\sum_{j}B^{\mathrm{f}}_{fj}\tilde{\tau}^{\mathrm{f}}_{ij} \quad (16)$$

$S^{D}_{u_i}$ is the added diffusion term that compensates for the added $a^{D}_{\mathrm{f}}u_{\mathrm{i-f}}$ on the lhs of Eq. (9) and is thus given by

$$S^{D}_{u_i}=-\sum_{\mathrm{f}}\mathrm{a}^{\mathrm{D}}_{\mathrm{f}}\left(u_{i-\mathrm{f}}-u_{i-\mathrm{P}}\right) \quad (17)$$

The last term on the rhs of Eq. (13) involves far-neighbour points which originate from the use of a second-order accurate linear upwind scheme (LUDS) as the interpolation scheme for the convective terms. With the linear upwind scheme used for the convective terms and central differences for diffusive terms, the coefficients a_{nb} become

$$a_{\mathrm{f}}=a^{D}_{\mathrm{f}}+a^{C}_{\mathrm{f}} \quad (18\ a)$$

where here f is the index of the cell neighbour to cell P accross face f. The convective coefficients a^{C}_{f} are assembled from the force fluxes (11) following standard expressions for the LUDS scheme which are also given in Pinto (1996). The diffusive coefficient of Eq. (18 a), based on a central-difference integration, is computed as

$$a^{D}_{f-nb}=\frac{\eta_{\mathrm{f}}}{V_{\mathrm{f}}}\left(B_{\mathrm{f}}\right)^2 \quad (18\ b)$$

where the scalar cell-face area is $B_{\mathrm{f}}=\sqrt{\sum_{j}B_{\mathrm{f}j}B_{\mathrm{f}j}}$ and the volume centered at the face f is calculated as $V_{\mathrm{f}}=\sum_{j}B_{\mathrm{f}j}\left[\Delta x_j\right]^{\mathrm{f}}_{f}$. The quantity $\left[\Delta x_j\right]^{\mathrm{f}}_{f}$ refers to a difference, calculated at face f, along direction $_f$ of component j of vector **x**, as follows

$$[\Delta x_j]_f^{\mathrm{f}} = x_j^{\mathrm{F}} - x_j^{\mathrm{P}},\ \text{e.g.,}$$

$$\text{for j= 2 and } f = 1,\ [\Delta x_2]_1^e = x_{2\mathrm{E}} - x_{2\mathrm{P}} \qquad (18\ \mathrm{c})$$

The central coefficient of the momentum Eq. (12-a) is given by

$$a_{\mathrm{P}} = \frac{\rho V_{\mathrm{P}}}{\delta \mathrm{t}} + a_o + S_{\mathrm{P}} \qquad (19)$$

with S_{P} the linearized part of the average value of the source ($S^{ui} = S_{ui} - S_P u_i$) over the control volume. S_{P} considers those terms of a general source multiplying $u_{i\text{-P}}$, and it also includes, for the LUDS scheme, the summation over the far-neighbour (ff) nodes ($\sum_{ff} a_{\mathrm{ff}}$)

The discretized stress equation has a similar outlook to the momentum Eq. (12 a)

$$a_{\mathrm{P}}^{\tau} \tau_{ij-\mathrm{P}} = \sum_f a_{\mathrm{f}}^{\tau} \tau_{ij-\mathrm{f}} + S_{\tau_{ij}} \qquad (20)$$

except for the absence of diffusive terms in the stress coefficients a_{f}. These coefficients are identical to those in the momentum equation (from 18) except that they need to be multiplied by λ/ρ, i.e., any

$$a_{\mathrm{f}} \text{ for stress} = \frac{\lambda}{\rho} a_{\mathrm{f}}^{C} \text{ for momentum} \qquad (21)$$

All the other contributions to the constitutive equation go to the source. The central coefficient of cell P is computed from Eq. (22) with near- and far-neighbour points in the summation due to the higher order scheme LUDS.

$$a_{\mathrm{P}} = \frac{V_P}{\delta t} + \sum_{\mathrm{f+ff}} a_{\mathrm{f}}^{\tau} \qquad (22)$$

The single cell volume V_{P} in Eq. (22) comes from the first term on the lhs of Eq. (8) and the source term is evaluated at the centre of a cell, as

$$S_{\tau_{ij}} = \eta_{\mathrm{P}} \left(\sum_l^3 \left(B_{ij}^{\mathrm{P}} [\Delta u_i]_l^{\mathrm{P}} + B_{li}^{\mathrm{P}} [\Delta u_j]_l^{\mathrm{P}} \right) \right) +$$

$$\lambda \sum_l^3 \sum_k^3 B_{lk}^{\mathrm{P}} \left(\tau_{ik} [\Delta u_j]_l^{\mathrm{P}} + \tau_{jk} [\Delta u_i]_l^{\mathrm{P}} \right) - \frac{2}{3} \eta_{\mathrm{P}} \left(\sum_l^3 \sum_k^3 B_{lk}^{\mathrm{P}} [\Delta u_k]_l^{\mathrm{P}} \right) \delta_{ij} \qquad (23)$$

Convective terms of the momentum and stress equations involve first derivatives of the quantities being convected, and thus lead to values of those quantities at the faces of the cells. These face values need to be computed from nodal values, a procedure which is based on an interpolation scheme. In this work the second order accurate linear upwind scheme, explained in Ferziger and Peric (1996), was used and the reader is also referred to Pinto (1996) for the equations for the convective coefficients.

The handling of the convective fluxes adopted here is based on the special interpolation scheme of Rhie and Chow (1982), with some modifications designed to avoid the problem of the final solution being dependent on the particular time-step used in the calculations, as explained in Issa and Oliveira (1994). Thus, the cell-face velocities ($\tilde{u}_{i-\mathrm{f}}$) are obtained and the wall fluxes are computed from (11), with the assurance that no pressure-velocity decoupling may occur.

3.2 Cell- Face Stresses

In the momentum equation it is necessary to compute the stresses at the cell faces from the stresses at nodal values, namel for the term (16) and there is a similar stress-velocity coupling problem, akin to the pressure-velocity coupling, that needs to be properly addressed. If a linear interpolation of nodal values of stress is used to compute face values, a possible lack of connectivity between the stress and velocity fields may result, and this can be solved by a practice inspired by that of Rhie and Chow (1982). Starting with Eq. (20) all terms are arithmetic-averaged to a particular cell-face f, except those multiplying velocity differences across the face (see Eq. 23), which are evaluated directly through

$$\overline{a_{\mathrm{P}}^{\tau} \tilde{\tau}_{ij}^{\mathrm{f}}} = \overline{H(\tau_{ij})} + \overline{b_{fj}} [\Delta u_i]_f^{\mathrm{f}} + \overline{b_{\mathrm{fi}}} [\Delta u_j]_f^{\mathrm{f}} +$$

$$\left(\overline{\sum_{l \neq f}^{2} b_{lj} [\Delta u_i]_l^{\mathrm{P}} + \sum_{l \neq f}^{2} b_{li} [\Delta u_j]_l^{\mathrm{P}}} \right) \qquad (24)$$

where $H(\tau_{ij})$ and the b- coefficients are defined as

$$H(\tau_{ij}) \equiv \sum_{nb} a_{nb}^{\tau} (\tau_{ij})_{\mathrm{nb}} \qquad (25)$$

$$b_{li} = \eta B_{li} + \lambda \sum_k^3 B_{lk} \tau_{ik} \qquad (26)$$

In Eq. (24) the velocity differences are evaluated according to the notation adopted and cell-centered ($[\Delta u]^{\mathrm{P}}$) and face-centered ($[\Delta u]^{\mathrm{f}}$) values must be carefully separated. It is computationally more efficient to use the face stress given by Eq. (27) below, obtained after arithmetic-averaging (20) and subtracting from (24), instead of Eq. (24) itself.

$$\tilde{\tau}_{ij}^{\mathrm{f}} = \frac{\overline{a_{\mathrm{P}}^{\tau} \tau_{ij}} + \overline{b}_{fj} [\Delta u_i]_f^{\mathrm{f}} + \overline{b}_{fi} [\Delta u_j]_f^{\mathrm{f}} - \left(\overline{b_{fj} [\Delta u_i]_f + b_{fi} [\Delta u_j]_f} \right)}{\overline{a_P^{\tau}}} \qquad (27)$$

The divergent of the stress term in the momentum equation, belonging to source $S_{ui\text{-stress}}$, (Eq. 18) should then be explicitly evaluated with the stresses on the cell faces.

3.3-The SIMPLEC Algorithm Extended to the Stress

The calculation of the pressure is carried out indirectly, since the momentum equation, where the pressure is explicitly present, is used for computing the velocity vector. Patankar and Spalding (1972) devised a method for calculating the pressure out of the continuity and a truncated momentum equations, known as the SIMPLE algorithm. Improvements to this philosophy have been developed in the following years and the SIMPLEC (SIMPLE consistent) algorithm introduced by Van Doormal and Raithby (1984) was adopted here and extended for the stress equation. This algorithm was originally developed for iterative time-marching, but here we adopt instead the time-marching version explained in Issa and Oliveira (1994).

The presence of a complex constitutive equation, after introducing the fictitious diffusion term, produces little changes upon the original SIMPLEC method, which is only concerned with the calculation of the pressure. Two new steps are introduced in the

SIMPLE-like algorithm to account for the stress equation and they are:

- the calculation of the stress tensor from the six implicit constitutive equations, which must be carried out just prior to the first time the three momentum equations are handled. Here the coefficients and source term are based on previous time-level velocity and stress values.
- Then, the momentum equations are solved implicitly for each velocity component with the stress obtained above going to the source term. The important step here is to base the divergence term (16) on the specially developed interpolation practice defined by (27). According to the standard pressure-correction approach, the pressure gradient term is based on previous time-level values and is singled out of the remaining source term for later use. The velocities obtained now do not satisfy the continuity equation and the algorithm proceeds as in the classical SIMPLEC case with further corrections of the velocity and pressure in order to satisfy momentum and mass continuity.

3.4- Boundary Conditions

At inlets the velocity field is known and given. The stress field depends of the velocity field, but since a general constitutive equation is implicit on the stress, further assumptions are required. For the particular flow configuration here considered, the inlet is far away upstream of the slip-stick junction and the velocity profile is uniform, thus leading to a zero stress field. The stress field will develop then as a consequence of the flow development.

The outlet is far away downstream of the region of interest, where profiles become approximately fully developed, so the values of velocity and stress at the outlet cells become exactly equal to those of the previous upstream cells.

For the symmetry planes fictitous cells may be created in which reflexion laws apply, thus defining the following boundary conditions at the cell-face f lying on the boundary:

- for the velocity component u_i

$$\left(u_i\right)^{\mathrm{P}} = \left(u_i\right)^{\mathrm{P}} - \left(u_n\right)^{\mathrm{P}} \cdot n_i \quad \text{with} \quad \left(u_n\right)^{\mathrm{P}} = \sum_j u_j^{\mathrm{P}} n_j \tag{28}$$

- for the pressure or other scalar quantity

$$p^{\mathrm{f}} = p^{\mathrm{P}} \tag{29}$$

As far as the stress field (τ_{ij}) is concerned that gives

$$\sum_k \left(\tau_{ik}\right)^{\mathrm{f}} n_k = \sum_k \left(\sum_j \left(\tau_{jk}\right)^{\mathrm{P}} n_j n_i\right) n_k \tag{30}$$

which is an implicit equation set on the unknown stress components on the boundary face ($\tau_{ik}{}^{\mathrm{f}}$). However, not each individual component of the stress tensor is required at f as deduced from inspection of the momentum equations. After integration on cell P the stress term in the momentum equation results

$$\left(S_{u_i-stress}\right)^{\mathrm{f}} = B_{\mathrm{f}} \sum_j \left(\tau_{ij}\right)^{\mathrm{f}} n_j \tag{31}$$

where the cell-face unit normal vector is computed from the area components as

$$n_j = \frac{B_{\mathrm{f}j}}{B_{\mathrm{f}}} \tag{32}$$

For solid walls the no-slip condition applies. i.e., using the fictituous cell one gets

$$(u_i)^{\mathrm{f}} = u_{i\mathrm{w}} \tag{33}$$

where $u_{i\text{-}w}$ is the wall velocity (here taken as zero).

As far as the pressure is concerned, its value at the wall is linearly extrapolated from the two nearest neighbour cells.

For the stress field the following wall boundary conditions apply for the case of a wall perpendicular to the i-direction

$$\tau_{ii} = 0, \tau_{jj} = -2\lambda\eta\left(\frac{\partial u_j}{\partial x_i}\right)^2, \ \tau_{ij} = -2\eta\frac{\partial u_j}{\partial u_i},$$

and

$$\tau_{kj} = -2\lambda\eta\frac{\partial u_k}{\partial u_i}\frac{\partial u_j}{\partial u_i} \quad \text{for } i \neq j \neq k \tag{34}$$

Note that in Eq. (34) the repeated indices summation rule does not apply.

NUMERICAL RESULTS AND DISCUSSION

4.1 Flow Conditions and Convergence Issues

The algorithm was applied to the solution of the entry flow problem of an Upper Convected Maxwell fluid (UCM) like that of Eggleton et al (1996). The model fluid properties were λ= 0.001 s, μ= 0.5 Pas and ρ= 1000 kg/m^3, and the channel half height (H) and inlet bulk velocity (U_{in}) were such that the Deborah (De) and Reynolds (Re) numbers of

$$De = \frac{\lambda U_{in}}{H} = 0.1$$

and

$$\mathrm{Re} = \frac{\rho U_{in} H}{\mu} = 20$$

were defined.

The two dimensional geometry outlined in Fig. 2 had an inlet length of 5 half-heights and an outlet length of 10 half-heights. The figure also defines the nomenclature used for the mesh size and the coordinate system. For purposes of mesh generation, the geometry was divided into two blocks, with block 1 in the wall-free region having NX_1 by NY cells patched to block 2 in the wall region with NX_2 by NY cells.

In order to assess the grid-size effect, various grids were defined but only the results pertaining to three of them (meshes 3, 5 and 7) are presented here. Characteristics of all grids are briefly presented in table I where f_x and f_y are geometrical factors used to concentrate nodes close to the wall leading edge.

Figures 3 a) and b) show axial profiles of the stress along a line (y/H=0.985) close to the symmetry plane and wall, normalised according to Eq. (35)

$$T_{ij} = \frac{\tau_{ij}}{\frac{\mu U_{in}}{H}} \tag{35}$$

The main feature of the flow is the large peak in all components of the stress as the flow approaches the wall. As far as grid refinement is concerned, with mesh 3 the flow is not yet grid independent, whereas the differences between the results from meshes 5 and 7 are only on the magnitude of the peak values of the

Table I- Summary of the main characteristics of the grids. δ_x^*, δ_y^* are the cell dimensions normalised by the channel half-height.

Grid	Block 1				Block 2			
	NX_1xNY	f_{x1}	f_{y1}	$\delta^*_{x,min}/\delta^*_{y,min}$	NX_2xNY	f_{x2}	f_{y2}	$\delta^*_{x,min}/\delta^*_{y,min}$
mesh 1	20 x 20	0.9131	0.95	0.1/ 0.03	40 x 20	1.0422	0.95	0.1/ 0.03
mesh 2	20 x 20	0.8712	0.95	0.05/ 0.03	40 x 20	1.0701	0.95	0.05/ 0.03
mesh 3	30 x 20	0.9085	0.95	0.03/ 0.03	60 x 20	1.0486	0.95	0.03/ 0.03
mesh 4	30 x 40	0.9085	0.9595	0.03/ 0.01	60 x 40	1.0486	0.9595	0.03/0.001
mesh 5	50 x 40	0.9293	0.9595	0.01/0.01	80 x 40	1.0505	0.9595	0.01/ 0.01
mesh 6	50 x 60	0.9293	0.9657	0.01/ 0.005	80 x 60	1.0505	0.9657	0.01/ 0.005
mesh 7	70 x 60	0.9428	0.9657	0.005/ 0.005	100 x 60	1.0465	0.9657	0.005/ 0.005

stress near the geometrical discontinuity. Far from the location of the slip-stick interface, there are no major differences between the various predictions and the flow development is independent of the mesh refinement, except for the three coarser grids of the table I.

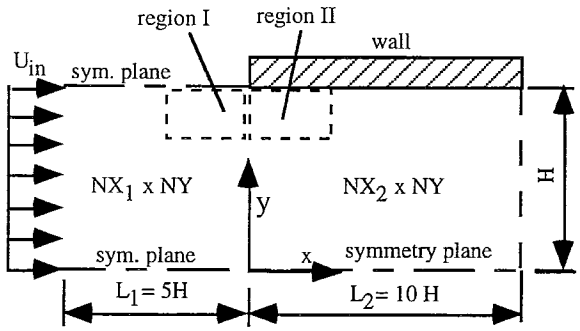

Figure 2- Schematic representation of the slip-stick geometry.

The current calculations were carried out with a much finer grid than those of Eggleton et al (1996) (their finest grid has a normalised spacing of 0.02). A comparison with their results close to the slip-stick junction is difficult because of the large scatter in their predictions. However, downstream of the junction, our calculations compare well with Eggleton et al's, as shown in the comparison of lateral profiles of two stress components at x/H=0.6 (Figs. 4-a and -b). Although these profiles are at a station some distance downstream from the wall leading edge, it can still be seen that the predictions with mesh 3 are slightly different than those with meshes 5 and 7, indicating that mesh 3 is inadequate to yield mesh-idependent results.

Still further downstream from the wall leading edge, the flow tends to a fully developed situation and our predictions of u_1, τ_{11} and τ_{12} at x/H=10 are undistinguishable from the theoretical profiles, thus giving some support to the coding of the UCM model in the original finite-volume program.

Viscoelasticity is responsible for convergence difficulties (Crochet, 1994) and this was no exception. For finer grids, convergence was found to be more difficult: for mesh 7 converged solutions could be obtained for Deborah numbers of 0.1 and 1.0 at a Reynolds number of 20, whereas for the coarser mesh 3 Deborah numbers in excess of 1.0 could be reached for the same Reynolds number, and Deborah numbers higher than 0.5 for a Reynolds number of 100, although with the first order accurate interpolation scheme known as the upwind differencing scheme. These limiting values are of the same order of magnitude as those found in the literature, pertaining to the same flow geometry (Eggleton et al, 1996). A more systematic study of the limits of convergence of the current method needs to be undertaken at different Reynolds numbers and the effect of the grid non-orthogonality should also be investigated.

The novel method devised to obtain the cell-face stresses (section 3.2) proved to be advantageous in more than one way. Its use coupled efficiently the velocity, pressure and stress fields, eliminating the oscilations found when the linear interpolation is used instead, as can be seen in the transverse profile of the transverse velocity component of Fig. 5. For the longitudinal velocity and stress tensor components similar effects to those seen in Fig. 5 were observed. The use of these special interpolation scheme also speeded up convergence in comparison to the linear scheme, with the decay of the residuals of the different equations being roughly 4 times as fast in the example of Fig. 5..

4.2 The Deborah number effect

The Deborah number effect was investigated in a comparison between the Newtonian flow case (De= 0.0) and the viscoelastic flow with a Deborah number of 0.1; in both cases mesh 7 and the linear-upwind scheme were used.

For this variation of the Deborah number changes of the mean flow pattern were rather small, as can be seen in the streamline plot of Fig. 6 a). However, an intense effect was encountered for higher Deborah numbers, as in the comparison between the Newtonian and De=1.0 flow cases of Fig. 6-b). Inspection of these and other figures not shown here show two different flow features which are worth mentioning: viscoelasticity causes a strong deviation of the fluid from the wall, thus creating a small layer depletied of fluid near the wall, in comparison to the Newtonian case; downstream of the slip-stick discontinuity, the viscoelastic flow aligns itself with the wall sooner than the Newtonian fluid flow case.

An understanding of these differences relies on the comparison between the Newtonian and viscoelastic fluid flow stress fields, corresponding to the Deborah numbers of Fig. (6-a). Countours of the normalised shear stress (T_{12}), longitudinal normal stress (T_{11}), transverse normal stress (T_{22}) and the first normal stress difference ($N_1= T_{11} - T_{22}$) are presented in Figs. 7 to 10, respectively. Their careful inspection shows that an element of Newtonian and non-Newtonian fluid is subjected to the stress fields schematically outlined in Fig. 11, in the two regions I and II. Note that the mesh is concentrated near the computational wall and the slight oscilations seen in the figure contours close to the symmetry plane (at bottom of figures) are a mere artifact of the contouring program together with the coarser mesh there.

In region I, components of the stress tensor for the Newtonian and the viscoelastic fluids have identical signs and similar

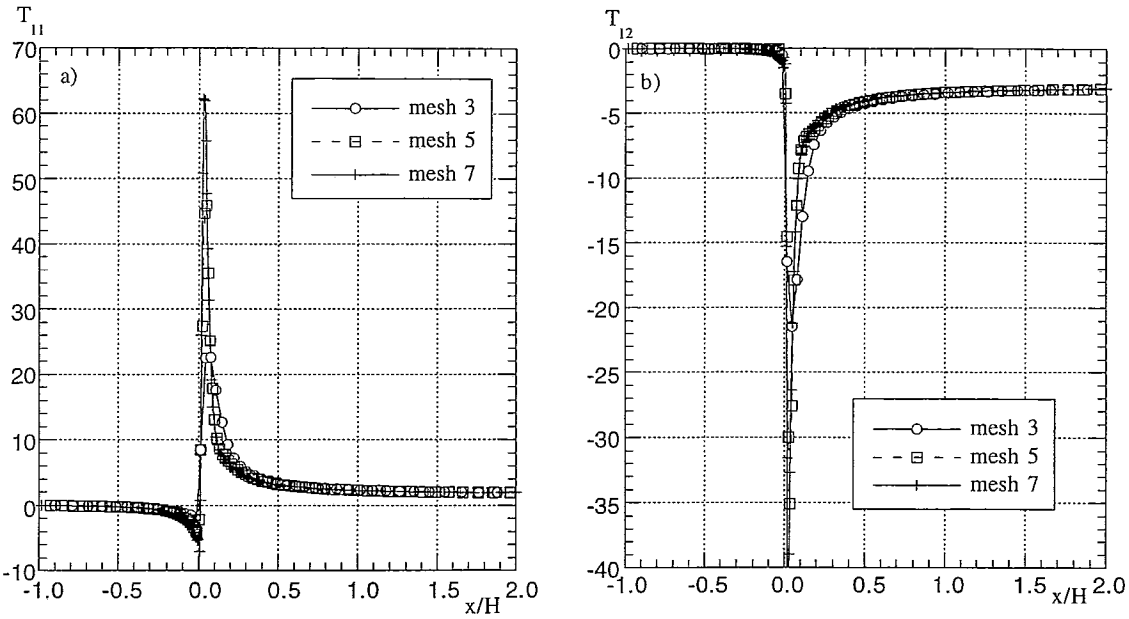

Figure 3- Effect of grid refinement on longitudinal profiles near the wall (Y/H= 0.985). a) Normalised axial normal stress (T_{11}). b) Normalised shear stress (T_{12}).

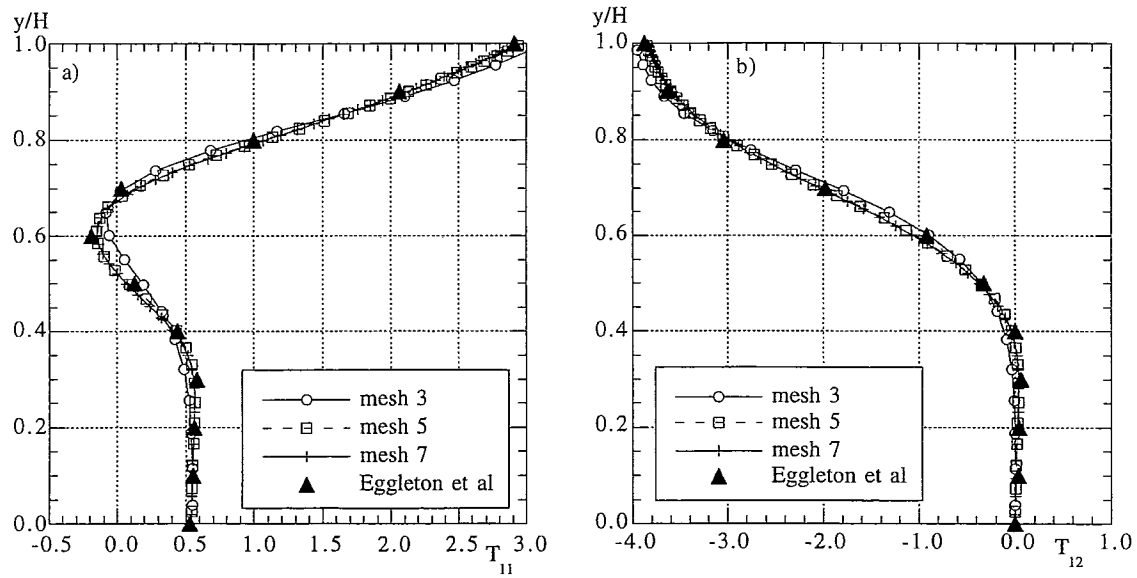

Figure 4- Comparison between the current predictions and those of Eggleton et al at x/H= 0.6. a) Transversal profile of the normalised axial normal stress b) Transversal profile of the normalised shear stress.

magitudes, except close to the wall leading edge where the non-Newtonian stresses reach much higher values. Similar stresses pertaining to the Newtonian fluid occur earlier in the flow than for the viscoelastic fluid, i.e., an element of Newtonian fluid is stressed further upstream than an element of viscoelastic fluid. All the components of the stress tensor act to deccelerate the flow and deviate it away from the symmetry plane, at y/H= 1 as the wall is approached: the building up of negative shear stress (Fig. 7) brakes the fluid flow as is typical of a situation where there is a wall at rest; a negative longitudinal normal stress (fig. 8) acts compressively thus retarding the flow longitudinally and simultaneously there is traction acting on the y-direction (positive T_{22}, Fig. 9), which forces the fluid away from the symmetry plane. So, the stress field acts upon both fluids in the same way, with similar stresses occuring further upstream for the Newtonian fluid. It should be emphasized that the identical qualitative contribution of the two normal stresses upon the flow translates into the summation of

their absolute values to compute the first normal stress difference, which is negative everywhere in region (Fig. 10).

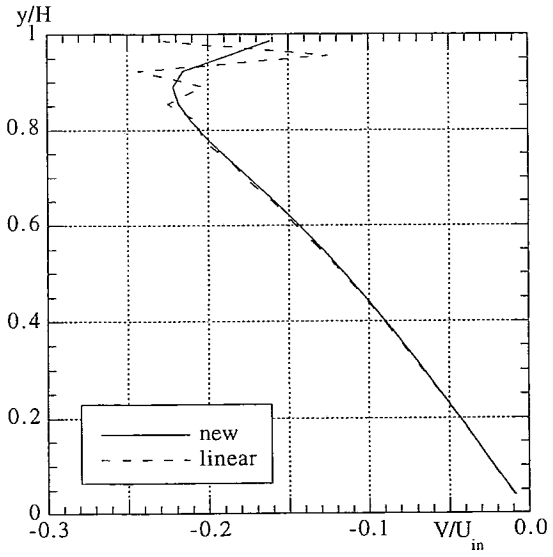

Figure 5- Comparison of transverse velocity components near the slip-stick boundary (x/H=-0.015, mesh 3) based on the linear and the new interpolation scheme for the stresses.

However, very close to the wall the viscoelastic fluid exhibits higher stresses and it is thus forced to deviate more from the wall than the Newtonian fluid as can be seen in the velocity profile of Fig. 12-a). For such a low elasticity fluid (De= 0.1) this effect can only be detected very close to the wall leading edge (inspect Fig. 6-a).

In region II a different situation arises: very close to the uncoming wall the shear stress (T_{12}) and the transverse normal stress (T_{22}) retain their directions, but are intensified, especially with the viscoelastic fluid. On moving downstream from the wall leading edge, the magnitudes of those two stresses quickly drop to similar levels, but a different behaviour is observed with the longitudinal normal stress (T_{11}). This stress is compressive (negative) for the Newtonian fluid but tractive (positive) and one order of magnitude higher for the viscoelastic fluid. Then, for the Newtonian fluid both normal stresses still act to deviate the fluid away from the wall, i.e., they both contribute negatively to the first normal stress difference, whereas an element of non-Newtonian fluid suffers a strong traction in the longitudinal direction, forcing the streamlines to align with the main flow direction. Figs. 8 and 9 show that T_{11} is much larger than T_{22} for the viscoelastic fluid, as reflected in the normal stress difference of Fig. 10, so, in spite of the tractive transverse normal stress acting to force the fluid away the from the wall the predominant effect is that of T_{11} and as a result the non-Newtonian flow becomes parallel to the wall faster than the Newtonian flow (see streamline plots of Fig. 6).

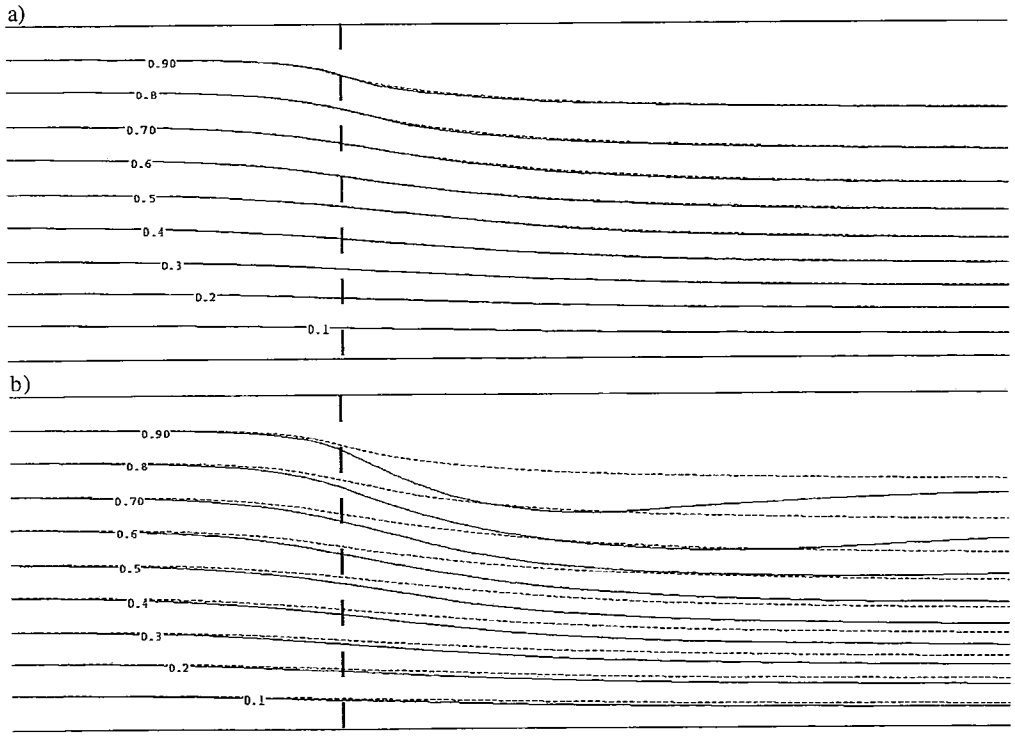

Figure 6- Streamlines for (a) De= 0 (dashed line) and De= 0.1 (full line); (b) De= 0 (dashed line) and De= 1.0 (full line). (zoom in the region x=-H to +2H) in mesh7 and Re= 20.

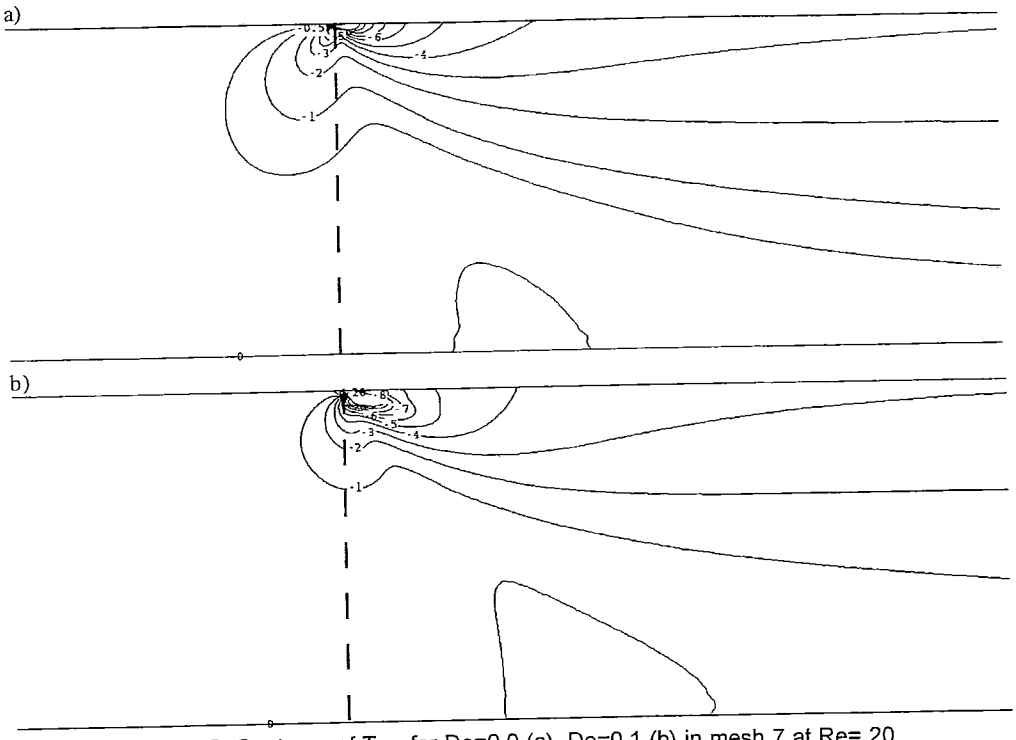

Figure 7- Contours of T_{12} for De=0.0 (a), De=0.1 (b) in mesh 7 at Re= 20

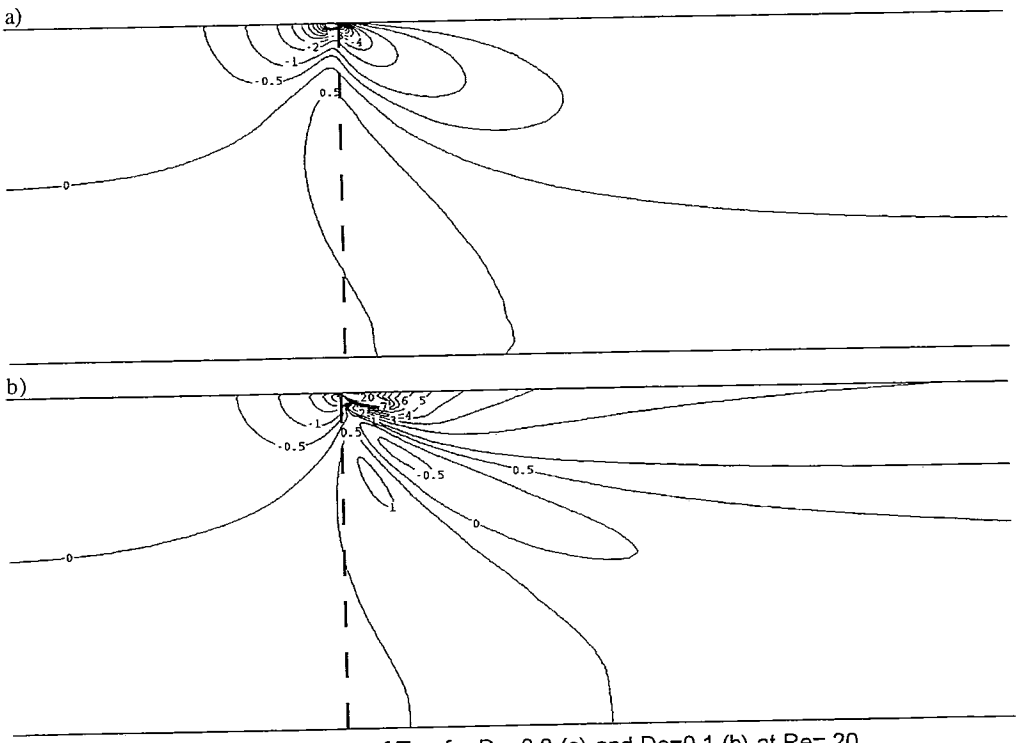

Figure 8- Contours of T_{11} for De=0.0 (a) and De=0.1 (b) at Re= 20.

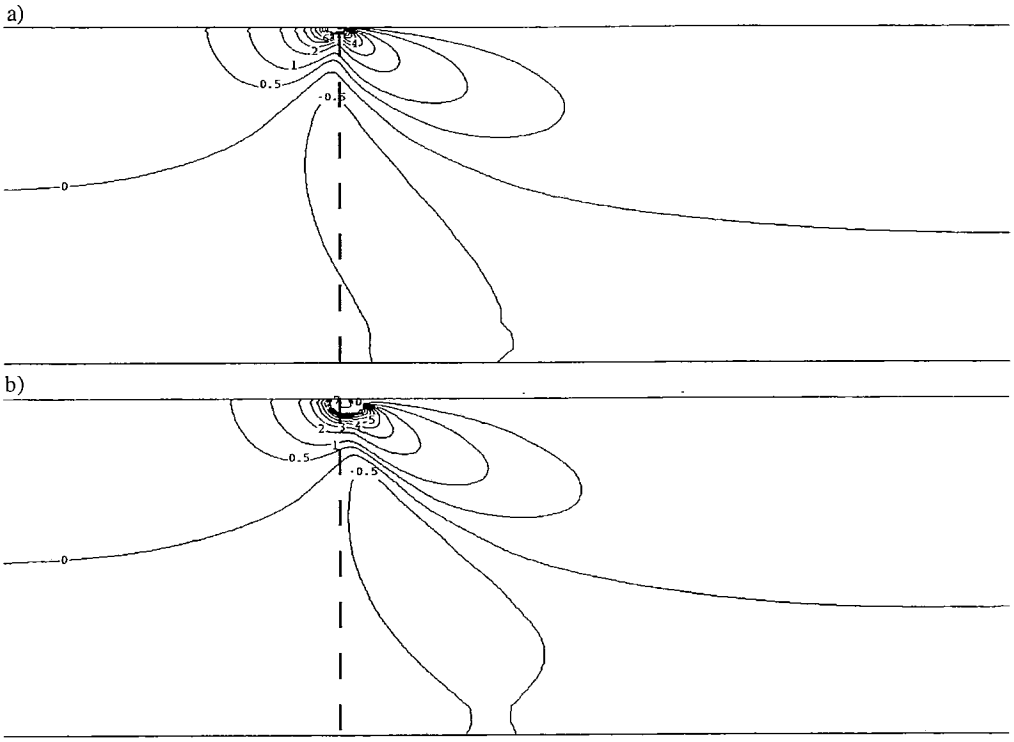

Figure 9 - Contours of T_{22} for De=0.0 (a) and De= 0.1 (b) at Re= 20.

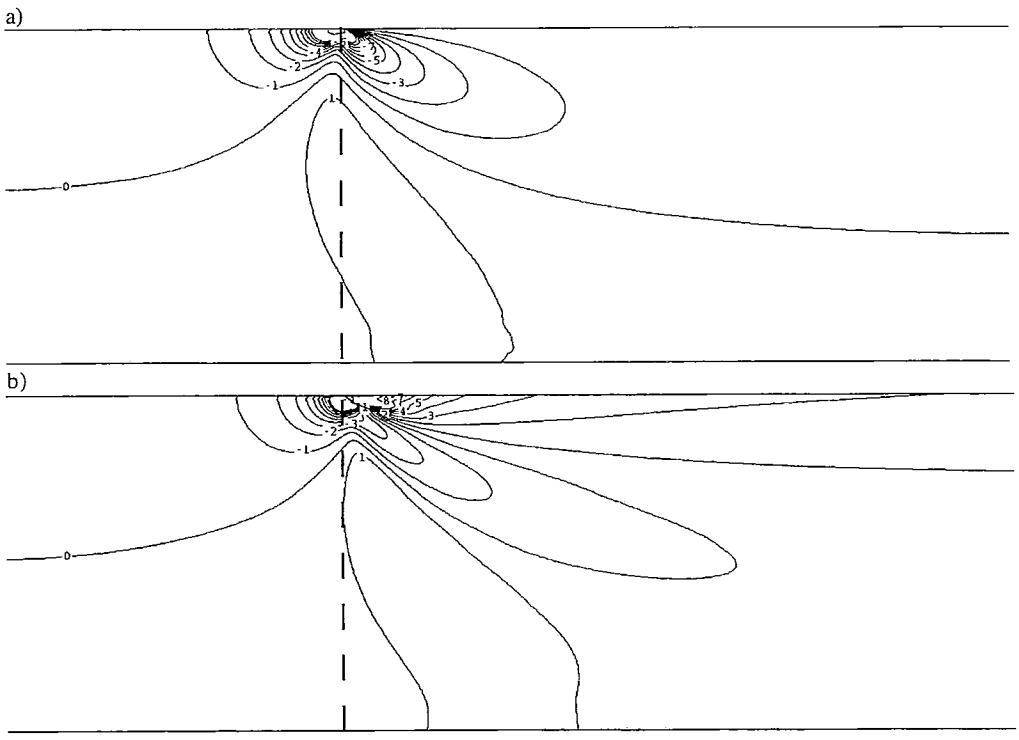

Figure 10- Contours of T_{11} - T_{22} for De=0.0 (a) and De= 0.1 (b) and Re= 20.

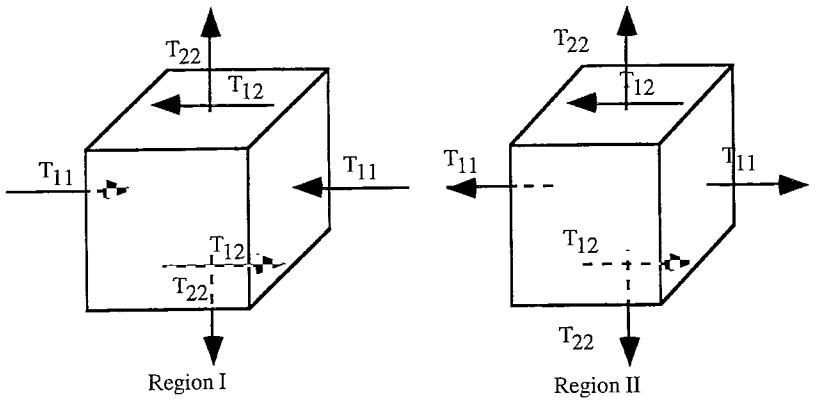

Figure 11 a)- Stress field acting upon an element of viscoelastic fluid (De= 0.1) in regions I and II of Fig. 3.

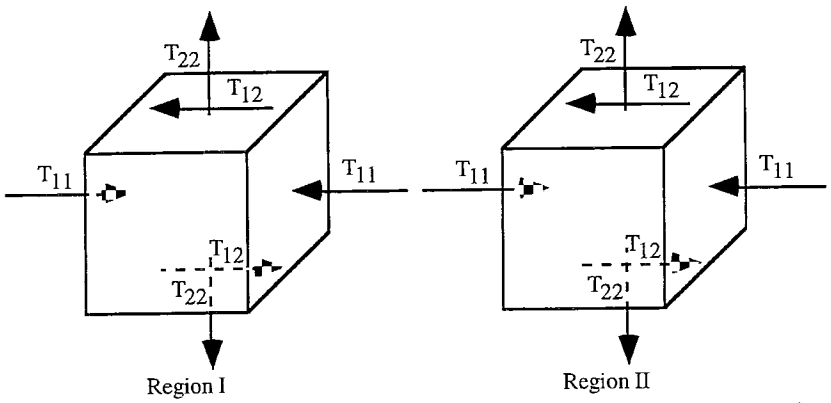

Figure 11 b)- Stress field acting upon an element of Newtonian fluid (De= 0.0) in regions I and II of Fig. 3.

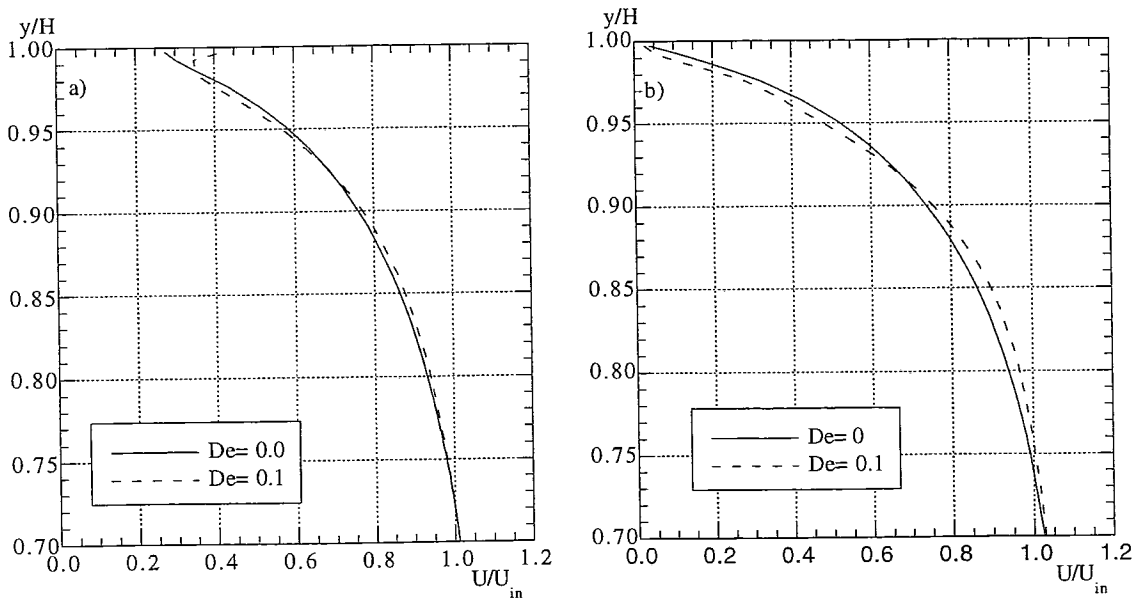

Figure 12- Transversal profiles of the axial velocity component in the vicinity of the slip-stick. Comparison between the De= 0.0 and De= 0.1 flows. a) x/H= -0.008. b)x/H= +0.031

The tractive force in the elastic flow case delays the effect of molecular diffusivity in the wall region, thus retarding flow development. The depletion of the viscoelastic fluid that happened just before the wall leading edge, within a small layer near the wall, has reduced the shear rates, and thus radial transfer of momentum in comparison to the Newtonian fluid case. The tractive force created by the normal stresses actually enhances this flow feature and as a consequence the velocity profile of Fig. 12-b) can be seen to have lower velocities close to the wall and a slightly fuller profile away from the wall. These effects upon the flow pattern are rather small because the Deborah number is low but are very much amplified by the fluid elasticity.

These comparisons were carried out for two flow configurations that do not differ significantly as far as the mean flow pattern is concerned, so the differences in the stress field can be attributed mainly to the new terms of the constitutive equation and is not affected by differences in the viscous term $2\eta\mathbf{D}$ in equation (3). This is also readily apparent by realizing that, due to continuity, $T_{11} = -T_{22}$ for the Newtonian fluid; now, from fig. 9 it is seen that T_{22} does not differ much between the two fluids, but T_{11} for De= 0.1 in zone II is completely different from T_{11} for De= 0.0 (Fig. 8). These differences can thus only be explained by the elastic terms in the constitutive equation.

For increased viscoelasticity the differences in flow pattern become rather large and though the viscous term may explain some of the differences in the stress field, the higher value of the time constant λ would then also lead to a much stronger effect of the new convective-like terms in the constitutive equation.

CONCLUSIONS

A new finite-volume methodology for the computation of the flow of viscoelastic fluids has been developed and is presented with some detail. The methodology is general in the sense that both 2-D and 3-D simulations can be performed and the finite-volume mesh may be non-orthogonal (and semi-structured) to conform to any arbitrary flow-boundary geometry.

The interpolation techniques used for all terms of the continuity, momentum and constitutive equations were second order accurate. The problem of the pressure- velocity- stress coupling was addressed and a new interpolation technique, inspired on Rhie and Chow's (1982) practice developed for Newtonian flows, was devised here for the stress terms appearing in the momentum equation.

Calculations for the channel entry flow of an upper convected Maxwell model at a Reynolds number of 20 and Deborah numbers of 0.1 and 1.0 were carried out to assess the performance of the programme; results for De= 0.1 were in good agreement with those of Eggleton et al (1996). Very fine computational meshes have been used, compared with those generally found in viscoelastic computations; the non-linear mesh spacing near the boundary discontinuity was 0.005 (compare with 0.02 in Eggleton et al work which used already a very fine mesh).

The grid refinement studies showed that the profiles of the calculated quantities were smooth (in contrast to Eggleton et al) and that grid independent values could be obtained except in the near vicinity of the wall discontinuity where stresses tended to infinity. The special interpolation technique developed for this work was seen to be effective in that no oscillations in the calculated quantities were detected and the convergence was faster than with a linear interpolation scheme. Convergence was attained for Deborah and Reynolds numbers identical to those reported in the literature for a similar flow problem using other numerical methods, namely for Deborah numbers in excess of 1.0 and 0.5 for a Reynolds number of 20 and 100, respectively.

The flow pattern at a Deborah number of 0.1 did not differ significantly from that of a Newtonian fluid and the viscoelastic fluids were seen to develop identical stresses much closer to the slip-stick boundary due to the retardation effect brought by the new elastic terms of the constitutive equation. However, as the wall was approached the viscoelastic fluid developed higher stresses thus being more effective in deviating the fluid away from the wall. In the developing flow region within the channel the longitudinal normal stress of viscoelastic fluids was seen to be tractive and very intense, whereas it was compressive and one order of magnitude smaller for Newtonian fluids, forcing the viscoelastic fluid to be more parallel to the wall counteracting the role of molecular diffusion. This, coupled with the previous depletion of fluid from the wall region has the effect of delaying flow redevelopment.

Further research is deemed necessary to understand the flow features very close to the wall discontinuity and deal with the very high stresses occuring in that place. Improvements in the performance of the model, especially in dealing with the stress boundary conditions and to increase its convergence range are also required. The effect of the non-orthogonality of the grid upon the behaviour of the model and its convergence rate also needs to be addressed in the future.

ACKNOWLEDGEMENTS

The authors acknowledge the financial support of project PBIC/P/QUI/1980/95 of JNICT without which this work could not have been carried out.

REFERENCES

Basara, B. and Younis, B. A. 1995. "Assessment of the SSG Pressure-Strain Model in Two-Dimensional Turbulent Separated Flows." J. Applied Scientific Res., vol. 55, 39-61.

Crochet, M. 1994. "Numerical simulation of viscoelastic flow." Lecture series 1994-03. Von Kárman Institute of Fluid Dynamics.

Eggleton, C. D., Pulliam, T. H. and Ferziger, J. H. 1996. "Numerical Simulation of Viscoelastic Flow Using Flux Differene Splitting at Moderate Reynolds numbers." J. Non-Newt. Fluid Mech., vol. 64, 269- 298.

Ferziger, J. H. and Peric, M. 1996 "Computational Methods for Fluid Dynamics." Springer Verlag, Berlin

Gaidos, R. E. and Darby, R. 1988. "Numerical simulation and change in type in the developing flow of a nonlinear viscoelastic fluid." J. Non-Newt. Fluid Mech., vol. 29, 59-79.

Gervang, B. and Larsen, P. S. 1991. "Secondary Flows in Straight Ducts of Rectangular Cross Section." J. Non-Newt. Fluid Mech., vol. 39, 217-237.

Hu, H. H. and Joseph, D. D. 1990. "Numerical Simulation of Viscoelastic Flow Past a Cylinder." J. Non-Newt. Fluid Mech., vol. 37, 347- 377.

Huang, X., Phan- Thien, N. and Tanner, R. I 1996. "Viscoelastic Flow between Eccentric Rotating Cylinders: Unstructured Control Volume Method." J. Non-Newt. Fluid Mech., vol. 64, 71-92.

Issa, R. I. and Oliveira, P. J. 1994. "Numerical predictions of phase separation in two-phase flow through T-junctions." Computers and Fluids, vol. 23, 347-372.

Khosla, P. K. and Rubin, S. G. 1974. "A Diagonally Dominant Second- Order Accurate Implicit Scheme." Computers and Fluids, vol. 2, 207.

Patankar, S. V. and Spalding, D. B. 1972. "A calculation procedure for heat, mass and momentum transfer in three-dimensional parabolic flows." Int. J. Heat and Mass Transfer, vol. 15, 1787.

Patankar, S. V. 1980. "Numerical Heat Transfer and Fluid Flow." McGraw-Hill, New York.

Peric, M. 1985. "A Finite-Volume Method for the Prediction of Three-Dimensional Fluid Flow in Complex Ducts." Phd Thesis, University of London, UK.

Pinto, G. A. 1996. "Development of a Numerical Simulation Programme for the Calculation of Laminar Flows with Non-Linear Elastic Fluids" (in portuguese). MSc. Thesis, University of Porto, Portugal.

Raithby, G. D. 1976. "A Critical Evaluation of Upstream Differencing Applied to Problems Involving Fluid Flow. " Comp. Meth. Appl. Mech. Eng., vol. 9, 75.

Rhie, C. M. and Chow, W. L. 1982. "A numerical study of the turbulent flow past an isolated airfoil with trailing edge separation." AIAA, vol. 82, 998.

Sasmal, G. P. 1995. "A Finite Volume Approach for Calculation of Viscoelastic Flow Through an Abrupt Axisymmetric Contraction." J. Non-Newt. Fluid Mech., vol. 56, 15-47.

Van Doormal, J. P.and Raithby, G. D. 1984. "Enhancements of the SIMPLE method for predicting incompressible fluid flows." Num. Heat Transfer, vol. 7, 147-163.

Versteeg,H. K. and Malalasekera, W. 1995. "An Introduction to Computational Fluid Dynamics", *The Finite Volume Method*, Longman Scientific & Technical

Xue, S.- C., Phan-Thien, N. and Tanner, R. I. 1995. "Numerical Study of Secondary Flows of Viscoelastic Fluid in Straight Pipes by an Implicit Finite Volume Method." J. Non-Newt. Fluid Mech., vol. 59, 192-213.

Yoo, J. Y. and Na, Y. 1991. "A Numerical Study of the Planar Contraction Flow of Viscoelastic Fluids Using the SIMPLER Algorithm." J. Non-Newt. Fluid Mech., vol. 39, 89-106.